Energy management of hybrid electric vehicles with battery aging considerations: Wheel loader case study

Iman Shafikhani and Jan Åslund

Shafikhani, I., Åslund, J., (2021), Energy management of hybrid electric vehicles with battery aging considerations: Wheel loader case study, *Control Engineering Practice*, 110, 104759.
https://doi.org/10.1016/j.conengprac.2021.104759

Energy management of hybrid electric vehicles with battery aging considerations: wheel loader case study

Iman Shafikhani[a,*], Jan Åslund[a]

[a] *Vehicular Systems Group, Department of Electrical Engineering, Linköping University, 58183 Linköping, Sweden*

Abstract

This paper presents a multi-objective energy management strategy for hybrid electric vehicles. It aims at reducing fuel consumption and minimizing battery wear simultaneously while fulfilling system's constraints. A control-oriented differential model is considered to account for battery aging effects and an algorithm is developed to identify its parameters. Energy management is formulated as an optimal control problem and is solved by Pontryagin's minimum principle. The controller is then implemented for a hybrid electric wheel loader to demonstrate its effectiveness. In short-term simulations for four drive cycles, behavior of the vehicle is compared to the case where energy management policy does not encompass battery wear minimization. Long-term simulations suggest that there is a huge potential in terms of extending battery life while the price to pay is a negligible increase in fuel consumption. It is observed that the proposed methodology works best for non-aggressive drive cycles.

Keywords: Energy, ECMS, Pontryagin, HEV, Aging

1. Introduction

Automotive market has witnessed a continuous surge in demand and production of hybrid electric vehicles (HEV), ever since the beginning of their mass production three decades ago. One of the key factors contributing to their attractiveness, besides other environmental and economical benefits, is less fuel consumption compared to their conventional counterparts. To ensure and maintain this, many researchers around the world have been successfully developing and applying energy management strategies (EMS) to optimize split of requested power between the on-board energy sources, namely fossil fuel and energy storage system (ESS), based on a wide spectrum of control engineering techniques (Onori et al., 2016; Sabri et al., 2016; Huang et al., 2017; Payri et al., 2014).

Dynamic programming (DP) and equivalent consumption minimization strategy (ECMS) are among the mostly studied methods in this regard. DP provides a globally optimal solution to the energy management problem by investigating all possible scenarios in a reverse-time manner (Pérez et al., 2006; Nüesch et al., 2014). Because of its high computational burden and requirement to access knowledge about future driving condition, DP is usually simulated offline and used as a benchmark to assess effectiveness of other methods. ECMS, on the other hand, is computationally efficient in that it amounts to instantaneous minimization of a cost function, which for a battery electric hybrid propulsion, is constructed by making fuel and battery powers comparable via concept of equivalence factor. According to its close ties with Pontryagin's minimum principle (PMP), which under certain conditions can yield a globally optimal solution to energy management problem (Kim and Rousseau, 2012), a properly designed ECMS can achieve results very close to those calculated by DP (Serrao et al., 2011a). Nevertheless, the assumption of knowing future driving information would still be a practical obstacle. Adaptive versions of ECMS have been developed to tackle this problem by determining equivalence factor as a function of operating conditions (Musardo et al., 2005; Onori et al., 2010; Sivertsson et al., 2011; Rezaei et al., 2017).

Earliest formulations of energy management problem were focused on reducing fuel consumption. However, performance of the designed policy is not to be assessed solely upon how much it improves fuel consumption, but also on several other factors such as its impacts on degradation of powertrain components. In particular, reduction in fuel consumption is achieved by recuperating power during regenerative braking and discharging battery to assist during traction phases, both of which accelerate processes that degrade battery in the long run (Spagnol et al.; Serrao et al., 2011b). Conversely, a battery-friendly policy would limit battery usage in both charge and discharge modes and automatically increases fuel expenditure. The compromise between the two can be formulated into a multi-objective optimization problem. In Ebbesen et al. (2012), this is done by considering dynamics of battery state of health in the optimal control problem, which augments the stan-

*Corresponding author

Email addresses: iman.shafikhani@liu.se (Iman Shafikhani), jan.aslund@liu.se (Jan Åslund)

dard ECMS by penalizing both charging and discharging modes of battery in order to reduced battery aging. Unfortunately, the trade-off between fuel consumption and battery health improvements is not explored. Given that temperature of battery system affects its degradation, authors in Padovani et al. (2013) have embedded temperature control into the energy management problem. The main issue is that high battery currents can accelerate battery wear regardless of temperature levels, which is not taken into account. Also, it is not illustrated, in quantitative terms, how the proposed temperature regulation prolongs battery health. Serrao et al. (2011b) makes fuel consumption and capacity degradation terms comparable in the cost function by turning them into equivalent monetary expenses according to battery's replacement costs. Effects of fuel price fluctuations is not considered in this work. This issue is resolved in Tang et al. (2014); Tang and Rizzoni (2016); Tang et al. (2015) by normalizing fuel mass flow rate and battery degradation terms with respect to their maximum values. Trade-off between the two objectives is studied by introducing a weighting penalty that varies from 0 to 1, which assigns a variable relative degree of importance to the objectives. The models used in the aforementioned articles are either from Wang et al. (2011) or Suri and Onori (2016), and in both cases it is not clear how to simulate the models when battery operating points are subject to variations. Pham et al. (2015) convexifies the empirical cycle life model presented in Wang et al. (2011) to derive analytical solution to a battery-life-optimizing energy management problem for hybrid trucks.

While development of optimal energy management policies for hybrid electric construction equipment is nothing new (Nilsson et al., 2015; Fröberg et al., 2011; Zhang et al., 2019), research on simultaneous optimization of fuel economy and energy storage system's durability is limited (Li et al., 2018). In this regard, to the best of the authors' knowledge, incorporation of battery degradation into energy management problem of hybrid electric wheel loaders and its potential advantages have not been studied yet. With this incentive in mind, the purpose of this paper is to propose a battery-friendly energy management methodology for hybrid electric vehicles. The structure considered for capacity loss model is based on the control-oriented model developed by Suri and Onori (2016) and the result of Petit et al. (2016), which suggests differentiation of batch models to simulate capacity loss for varying operating conditions. A two-stage algorithm is presented to identify the aging model parameters based on constant C-rate experiments' data. The energy management problem is formulated within optimal control framework and is solved by Pontryagin's minimum principle. With some simplifications, the proposed controller is implemented for a series hybrid electric wheel loader and its performance in achieving energy management's objectives is assessed.

The paper is organized as follows. In section 2, models of the key components are described, and an algorithm is proposed to identify parameters of the battery's capacity loss model. Section 3 is dedicated to discussing choice of the multi-objective cost function and formulating the energy management problem. Solution to the optimal control problem and the corresponding implementation for the hybrid wheel loader are given in section 4 and 5, respectively. In section 6, short-term and long-term simulation results are presented and controller's performance is evaluated. Section 7 concludes the paper with future research directions.

2. Vehicle model description

The hybrid vehicle under consideration is the Volvo's series hybrid electric wheel loader LX1. A basic schematic of the powertrain is shown in figure (1). The transmission system allows for full electric drive, hybrid drive, battery recharging and regenerative braking modes. At any given moment, mechanical power requested from driver is translated into electric power at the output of the inverter, and has to be met by the battery system in conjunction with serial connection of combustion engine and generator. Distribution of power request between the two energy routes is governed by the energy management control system. The controller has to ensure fulfillment of power demand while optimizing a specific cost function. Basic descriptions of relevant components is given in the sequel.

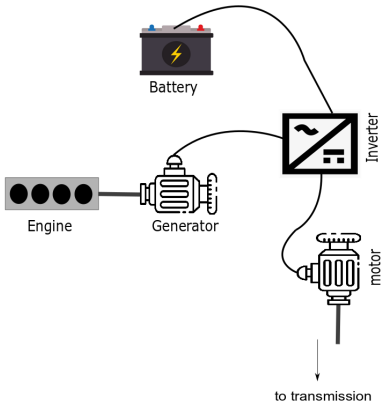

Figure 1: Series hybrid configuration

2.1. Genset

In the series hybrid architecture shown in figure (1), genset (or generator set) is a serial connection of a diesel engine and an electric machine. For the present study, Willans approximations are used for both components. Such models are simplified versions of measured maps, and are derived by linearly approximating a characterizing equation of the component (Guzzella et al., 2007). Model for the electric machine is given as a map

$$P_{elec} = f_{em}(\omega, T_{em}), \tag{1}$$

where P_{elec} is the electric power of the electric machine, T_{em} is the torque, ω is the rotational speed of the shaft, and f_{em} represents the map. The electric machine can operate as motor to enable engine braking so as to limit battery charging during regenerative braking phases. Similarly, the model for the engine is given by the following mapping.

$$P_{fuel} = f_{ice}(\omega, T_{ice}), \tag{2}$$

P_{fuel} is the fuel power corresponding to the engine torque T_{ice} and the speed ω. Neglecting the parasitic torque, the genset dynamics is

$$T_{ice} + T_{em} = J_e \dot{\omega}, \tag{3}$$

in which J_e is the shaft's inertia. For energy management problem at hand, this fast dynamics can be neglected and it suffices to approximate genset model by a static map, which associates an optimal fuel consumption to any admissible output electric power request. In other words, for every admissible electric power demanded from genset, engine's operating points are chosen such that fuel consumption becomes minimum, while fulfilling the power request. The resulting model is shown in figure (2). Here it is assumed that when the power request is zero, the engine is switched off and hence no fuel is consumed. The static map can be approximated by a linear function (for positive demands) described by

$$P_f = \begin{cases} P_{f,0} + \gamma P_{elec}, & \text{if } P_{elec} > 0 \\ 0, & \text{otherwise}, \end{cases} \tag{4}$$

in which P_f is minimal fuel power, $P_{f,0}$ is the fuel power at idling, P_{elec} is generator's electric power and γ is the slope of the approximated straight line.

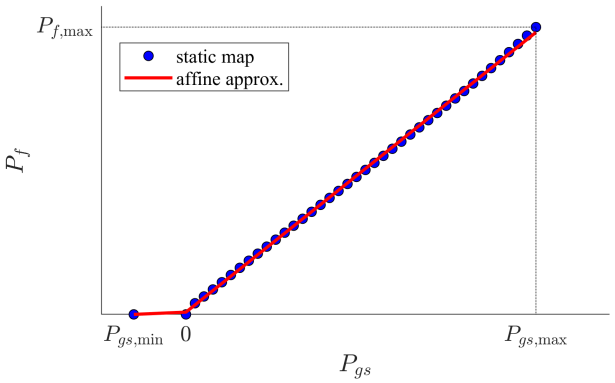

Figure 2: genset static model. P_{gs} is the electric power required from/ provided to the genset. Minimum and maximum values of genset's output power are denoted by $P_{gs,\min}$ and $P_{gs,\max}$, respectively.

2.2. Battery

The battery system is composed of series and parallel-connected commercial $LiFePO_4$ cells with cell capacity of 14 Ah each. The steady-state behavior of the battery is modeled by equivalent circuit model with open circuit voltage U_{oc} and inner resistance R_{eq}, shown in figure (3). Terminal power is $P_b = V_b I_b$ and the current is calculated by

$$I_b = \frac{U_{oc} - \sqrt{U_{oc}^2 - 4RP_b}}{2R}. \tag{5}$$

State of charge (SOC) is defined as the available electric

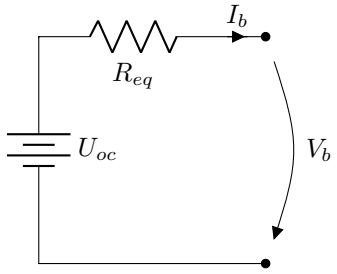

Figure 3: Equivalent circuit model of the battery.

charge relative to the battery's maximum capacity at the time under consideration:

$$\text{SOC} = \frac{Q}{Q_{\max}} \tag{6}$$

Consider $Q_{\max}$ to remain constant through usage, i.e. there is no battery wear. Then, battery dynamics is given by

$$\dot{\text{SOC}} = -\frac{I_b}{Q_{\text{rated}}} \tag{7}$$

in which I_b is battery current and Q_{rated} is the nominal battery capacity. Sign convention is taken such that positive and negative currents correspond to discharge and charge of battery, respectively.

As battery degrades through usage (cycle aging) and/or due to aging processes that are functions of time (calendar aging), maximum capacity $Q_{\max}$ fades and state of charge increases for the same value of available electric charge Q. In this case, instead of using SOC, available electrochemical energy of the battery ($W_{ech} = Q \times U_{oc}$) is taken as the system state. The corresponding dynamics is (Fröberg et al., 2011)

$$\dot{W}_{ech} = -\frac{P_b}{0.5 + \sqrt{0.25 - R_{eq}\frac{P_b}{U_{oc}^2}}}. \tag{8}$$

Battery degradation manifests itself as capacity fade, power fade and other effects such as stress-strain effects, etc. To improve battery life as an objective of energy management problem, it is crucial to develop and utilize accurate-enough models of such phenomena. Once a model that quantifies aging effects on important battery parameter(s) based on battery's operating points is found, it can be directly integrated into cost function of the optimization problem. In this work, incorporation of battery

life into energy management problem is done by penalizing capacity fade of the battery, which calls for a decent control-oriented aging model.

Electrochemical degradation models, often represented by coupled partial differential equations, are built based on physics and chemistry of what happens inside the battery. Regarding accuracy of prediction, such models outperform empirical and semi-empirical models that predict cell wear without extensive understanding of physics of the cell. This is achieved at the expense of significant increase in model structure complexity and reduction in speed of simulation (Jin et al., 2018), which makes them a poor choice for control purposes. In order to design a control policy that compensates for battery wear, it is paramount that aging models are simple enough while at the same time they capture primary effects of factors such as state of charge, current, temperature, etc. One such model, presented in Wang et al. (2011), is found by using a *test matrix* composed of constant C-rate (I_c), constant temperature (θ) symmetric discharge/charge cycle tests shown in figure (4). C-rate is defined as absolute value of battery current in ampere divided by battery capacity in ampere-hour (Ah), i.e.

$$I_c = \frac{|I_b(\mathrm{A})|}{Q_{\max}(\mathrm{Ah})} \tag{9}$$

The model is given by

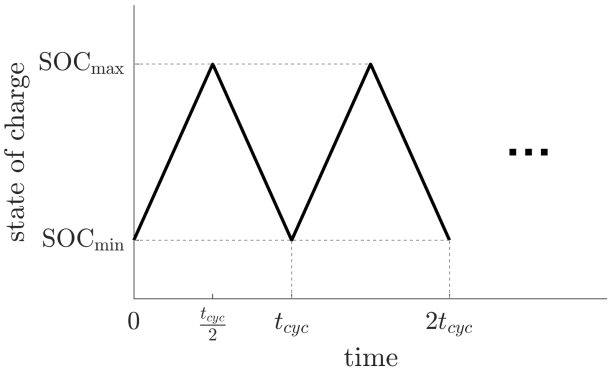

Figure 4: Symmetric load cycle for identification of battery aging model. $t_{cyc} = 2 \times \frac{\mathrm{SOC}_{\max} - \mathrm{SOC}_{\min}}{I_c}$ is the duration of one full cycle

$$Q_{loss} = B \cdot \exp\left(\frac{-E_a}{R_{gas}\theta}\right) \mathrm{Ah}^z, \tag{10}$$

where $E_a = 31500$ is the activation energy, $R_{gas} = 8.314$ (J/mol.K) is the gas constant, θ is the battery packs' temperature in Kelvin, $\mathrm{Ah} = \int_0^t |I(\tau)|d\tau$ is the Ah-throughput (t is in *hours*), B is a constant and Q_{loss} is capacity loss in ampere-hour. This model, however, does not include expected effects of state of charge. Another model proposed by Suri and Onori (2016) captures this dependency and gives capacity loss in percentage:

$$\begin{aligned} Q_{loss\%} &= 100 \cdot \frac{Q_{\max}(0) - Q_{\max}(t)}{Q_{\max}(0)} \\ &= (\alpha \mathrm{SOC} + \beta) \cdot \exp\left(\frac{-31700 + 163.3 I_c}{R_{gas}\theta}\right) \cdot \mathrm{Ah}^z \end{aligned} \tag{11}$$

In (11), $Q_{\max}(0)$ is the rated capacity (or equivalently, maximum cell capacity at $t = 0$), $Q_{\max}(t)$ is maximum capacity at time t and (α, β) depend on SOC. This model is found through similar loading cycles as the model (10). State of charge is not constant during these cycles and hence SOC in (11) represents the average value it takes through the cycle. Simplicity of this model makes it a proper candidate to be incorporated into energy management formulation (Tang et al., 2015), but it is not clear how to simulate it when battery operating points fluctuate a lot. The aim is basically to obtain an estimate for how much battery degrades during a small-enough interval if battery's operating points during the interval and maximum capacity at the beginning of the interval are known, i.e. given $Q_{\max}(t)$, current $I_{\mathcal{I}}$, temperature $\theta_{\mathcal{I}}$, and state of charge $\mathrm{SOC}_{\mathcal{I}}$, where $\mathcal{I}_{t,\delta t} = [t, t + \delta t]$ and δt is small, how to find a rough estimate for $Q_{\max}(t + \delta t)$. The aging model will then be used to simulate maximum capacity for varying operating points by adding up individual contributions of each small interval. It is clear that (11) cannot be used directly in this manner since dependency on time is not linear ($Q_{loss\%} \sim t^z$) and the result would be very sensitive to the choice of δt, but it can be used to investigate how the interval $\mathcal{I}$ contributes to degradation for symmetric, constant C-rate discharge/charge cycles. Define $Q_{loss}(t) \coloneqq Q_{\max}(0) - Q_{\max}(t)$, $\alpha' \coloneqq 0.01 Q_{\mathrm{rated}} \alpha$, and $\beta' \coloneqq 0.01 Q_{\mathrm{rated}} \beta$ to rewrite (11) as

$$\begin{aligned} Q_{loss}(t) = (\alpha' \mathrm{SOC} + \beta') \exp\left(\frac{-31700 + 163.3 I_c}{R_{gas}\theta}\right) \\ \cdot \left(\int_0^t |I(\tau)|d\tau\right)^z \end{aligned} \tag{12}$$

Taking both sides of (12) to the power of $\frac{1}{z}$ yields

$$\begin{aligned} Q_d(t) = (\alpha' \mathrm{SOC} + \beta')^{\frac{1}{z}} \exp\left(\frac{-31700 + 163.3 I_c}{R_{gas}\theta z}\right) \\ \cdot \int_0^t |I(\tau)|d\tau \end{aligned} \tag{13}$$

in which $Q_d(t) \coloneqq Q_{loss}^{1/z}(t)$. From (13),

$$Q_d(t + \delta t) = Q_d(t) + \mathcal{A}(\mathrm{SOC}, I, Q_{\max})\delta t \tag{14a}$$

$$Q_{\max}(t + \delta t) = Q_{\mathrm{rated}} - Q_d(t + \delta t)^z \tag{14b}$$

in which $\mathcal{A}(\mathrm{SOC}, I, Q_{\max})$ is defined as the *aging intensity factor* corresponding to the interval $\mathcal{I}_{t,\delta t} = [t, t + \delta t]$ and

is defined by

$$\mathcal{A}(\mathrm{SOC}, I, Q_{\max}) \coloneqq (\alpha' \mathrm{SOC} + \beta')^{\frac{1}{z}} \cdot \exp\left(\frac{-31700 + 163.3\frac{|I|}{Q_{\max}}}{R_{gas}\theta z}\right)|I(t)| \quad (15)$$

From (15), $\mathcal{A}(\mathrm{SOC}, I, Q_{\max})$ can be regarded as contribution of $\mathcal{I}_{t,\delta t}$ to degradation. Continuous form of (14) is obtained by computing ${}^{(Q_d(t+\delta t) - Q_d(t))}/_{\delta t}$ and taking the limit as $\delta t \to 0$. The resulting differential algebraic equation (DAE) becomes

$$\dot{Q}_d(t) = \mathcal{A}(\mathrm{SOC}, I, Q_{\max}) \quad (16a)$$

$$Q_{\max}(t) = Q_{\mathrm{rated}} - Q_d(t)^z \quad (16b)$$

with initial conditions $Q_d(0) = 0$, $Q_{\max}(0) = Q_{\mathrm{rated}}$. The approach taken so far is similar to differentiating (12) with respect to time. Similar idea is used in Prada and Petit (2013); Sciarretta et al. (2014), but the differentiated models do not include dependency on state of charge. In Petit et al. (2016), it is demonstrated that the differentiation approach can be useful for cases where battery undergoes cycles with varying operating points. Similarly, the DAE (16) is used directly, instead of the original model (11), to model capacity fade for constant C-rate discharge/charge cycles. A comparison between predictions of the models (11) and (16) is shown in figure (5)).

For the present application, battery cells' temperature is kept constant via an independent controller. (16) is hence employed for capacity fade prediction in situations where state of charge and current vary freely. Identification of the model's parameters is performed using a collection of constant C-rate discharge/charge cycles with different SOC ranges and C-rates. Even though C-rate is constant in all experiments, magnitude of current changes due to reduction in maximum capacity (see definition (9)).

2.2.1. Identification of the aging model

Suppose that N number of constant C-rate experiments characterized by SOC trajectories as in figure (4) are available. Assume that for the jth experiment, a vector of maximum cell capacities $\bar{\mathcal{Q}}^{(j)} = [\mathcal{Q}_0^{(j)}, \mathcal{Q}_1^{(j)}, \ldots, \mathcal{Q}_{r_j}^{(j)}]^T$ in descending order, a vector with number of cycles completed $\bar{n}^{(j)} = [n_0^{(j)}, n_1^{(j)}, \ldots, n_{r_j}^{(j)}]^T$, C-rate $I_c^{(j)}$, and minimum/maximum state of charge ($\mathrm{SOC}_{\min}^{(j)}$, $\mathrm{SOC}_{\max}^{(j)}$) are given. Entries of $\bar{\mathcal{Q}}^{(j)}$ and $\bar{n}^{(j)}$ respectively correspond to maximum capacity measurements and total number of cycles completed at time instances $\bar{t}^{(j)} = [t_0^{(j)}, t_1^{(j)}, \ldots, t_{r_j}^{(j)}]^T$, in chronological order, via $r_j + 1$ number of consecutive reference performance tests (RPT)(Groot, 2012), where r_j is large enough. By default, $\mathcal{Q}_0^{(j)} = Q_{\mathrm{rated}}^{(j)}$, $n_0^{(j)} = 0$ and $t_0^{(j)} = 0$. Denote the $k^{(j)}$th interval by $\mathcal{I}_k^{(j)} = [t_{k-1}^{(j)}, t_k^{(j)}]$, $k = 1, 2, \ldots, r_j$, and the $l^{(j)}$th cycle by $\mathcal{C}_l^{(j)}$.

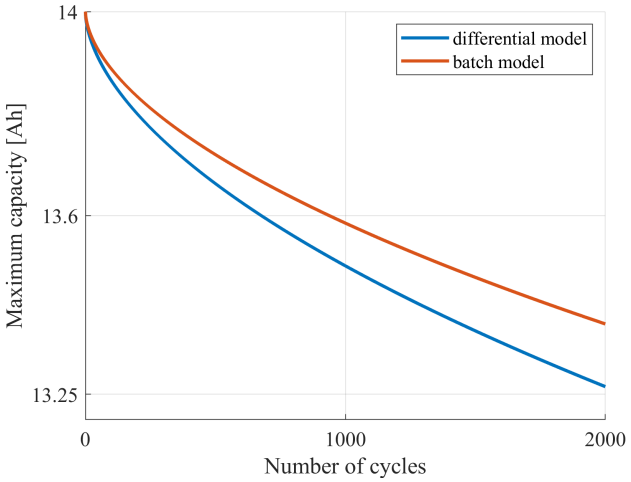

Figure 5: Comparison between batch model (11) (red line) and differential model (16) (blue line) maximum capacity predictions for a constant C-rate loading cycle ($I_c = 4$, $\mathrm{SOC}_{\min} = 0$, $\mathrm{SOC}_{\max} = 1$, $\theta = 30^{\circ}\mathrm{C}$)

The model to be identified is

$$\dot{Q}_d(t) = (\alpha' \mathrm{SOC} + \beta')^{\frac{1}{z}} \exp\left(\frac{-31700 + \zeta\frac{|I|}{Q_{\max}}}{R_{gas}\theta z}\right)|I(t)| \quad (17a)$$

$$Q_{\max}(t) = Q_{\mathrm{rated}} - Q_d(t)^z \quad (17b)$$

and the objective is to find the parameters $(\alpha', \beta', \eta, z)$. It is assumed that ζ and z are constants, and α' and β' are piecewise constant functions of SOC. From (17),

$$\begin{aligned}\dot{Q}_{\max} &= -zQ_d^{z-1}\dot{Q}_d \\ &= -z(Q_{\mathrm{rated}} - Q_{\max})^{(1-\frac{1}{z})}(\alpha' \mathrm{SOC} + \beta')^{\frac{1}{z}} \\ &\quad \cdot \exp\left(\frac{-31700 + \zeta\frac{|I|}{Q_{\max}}}{R_{gas}\theta z}\right)|I(t)|\,. \end{aligned} \quad (18)$$

(18) can be written in the differential form

$$\frac{\mathrm{d}Q_{\max}}{(Q_{\mathrm{rated}} - Q_{\max})^{(1-\frac{1}{z})}} = -z(\alpha' \mathrm{SOC} + \beta')^{\frac{1}{z}} \cdot \exp\left(\frac{-31700 + \zeta\frac{|I|}{Q_{\max}}}{R_{gas}\theta z}\right)|I(t)|\mathrm{d}t. \quad (19)$$

Integrating (19) over $\mathcal{I}_k^{(j)}$, assuming equal magnitudes for charge and discharge C-rates, i.e. $I_{c,\mathrm{ch}}^{(j)} = I_{c,\mathrm{dis}}^{(j)} = I_c^{(j)}$, yields

$$\int_{\mathcal{Q}_{k-1}^{(j)}}^{\mathcal{Q}_k^{(j)}} \frac{\mathrm{d}Q_{\max}}{(Q_{\mathrm{rated}} - Q_{\max})^{(1-\frac{1}{z})}} = -z\exp\left(\frac{-31700 + \zeta I_c^{(j)}}{R_{gas}\theta z}\right) \cdot \int_{t_{k-1}^{(j)}}^{t_k^{(j)}} (\alpha' \mathrm{SOC} + \beta')^{\frac{1}{z}}|I|\mathrm{d}t \quad (20)$$

Note that the exponential term is taken out from the integral since both $I_c = \frac{|I|}{Q_{\max}}$ and θ are constant during experiments. Left-hand-side of (20) amounts to

$$z\left[(Q^{(j)}_{\text{rated}} - \mathcal{Q}^{(j)}_{k-1})^{\frac{1}{z}} - (Q^{(j)}_{\text{rated}} - \mathcal{Q}^{(j)}_{k})^{\frac{1}{z}}\right] \tag{21}$$

The integral term in the right-hand-side of (20) is the summation of the integral taken over each discharge/charge cycle, i.e.

$$\int_{t^{(j)}_{k-1}}^{t^{(j)}_{k}} (\alpha'\text{SOC}+\beta')^{\frac{1}{z}}|I|\,\mathrm{d}t = \sum_{l=n^{(j)}_{k-1}+1}^{n^{(j)}_{k}} \oint_{\mathcal{C}^{(j)}_{l}} (\alpha'\text{SOC}+\beta')^{\frac{1}{z}}|I|\,\mathrm{d}t \tag{22}$$

Maximum capacity is fairly constant during one cycle. Accordingly, the integral in the summation can be written

$$\begin{aligned}\oint_{\mathcal{C}_l(j)} (\alpha'\text{SOC}+\beta')^{\frac{1}{z}}|I|\,\mathrm{d}t &= \oint_{\mathcal{C}^{(j)}_{l}} (\alpha'\text{SOC}+\beta')^{\frac{1}{z}}|I_c|Q_{\max}\,\mathrm{d}t \\ &\approx |I^{(j)}_c|Q^{(j)}_{l,\max} \oint_{\mathcal{C}^{(j)}_{l}} (\alpha'\text{SOC}+\beta')^{\frac{1}{z}}\,\mathrm{d}t \end{aligned} \tag{23}$$

in which $Q_{l,\max}$ is the average maximum capacity during $l^{(j)}$th cycle. From figure (4), it is straightforward to calculate $\oint_{\mathcal{C}^{(j)}_{l}} (\alpha'\text{SOC}+\beta')^{\frac{1}{z}}\,\mathrm{d}t$, with the assumption that α' and β' are constant for $\text{SOC} \in [\text{SOC}^{(j)}_{\min}, \text{SOC}^{(j)}_{\max}]$.

$$\begin{aligned}\oint_{\mathcal{C}^{(j)}_{l}} (\alpha'\text{SOC}+\beta')^{\frac{1}{z}}\,\mathrm{d}t &= 2\int_{\text{charge}} (\alpha'\text{SOC}+\beta')^{\frac{1}{z}}\,\mathrm{d}t \\ &= 2\int_{\text{charge}} (\alpha'\text{SOC}_{\min}+\beta'+\alpha'|I_c|t)^{\frac{1}{z}}\,\mathrm{d}t \\ &= \frac{2z}{(z+1)\alpha'^{(j)}|I^{(j)}_c|}[(\alpha'^{(j)}\text{SOC}^{(j)}_{\max}+\beta'^{(j)})^{\frac{1}{z}+1} \\ &\quad - (\alpha'^{(j)}\text{SOC}^{(j)}_{\min}+\beta'^{(j)})^{\frac{1}{z}+1}] \end{aligned} \tag{24}$$

In (24), $(\alpha'^{(j)}, \beta'^{(j)})$ designates values of (α, β) for $\text{SOC} \in (\text{SOC}^{(j)}_{\min}, \text{SOC}^{(j)}_{\max})$. For two different experiments, $(\alpha'^{(i)}, \beta'^{(i)})$ are not necessarily equal. If α' and β' are not constant for the cycle's SOC window, corresponding expressions as in (24) can be found by decomposing the integral into several windows of each having constant α' and β'. Naturally, considering more values for each of these parameters as functions of SOC requisites more diverse experiments in terms of ($\text{SOC}_{\min}$,$\text{SOC}_{\max}$). Now from (22-24), the right-hand-side of (20) is approximately

$$\begin{aligned}&-\exp\left(\frac{-31700+\zeta I^{(j)}_c}{R_{gas}\theta z}\right)\frac{2z^2}{(z+1)\alpha'^{(j)}}\sum_{l=n^{(j)}_{k-1}+1}^{n^{(j)}_{k}} Q^{(j)}_{l,\max} \\ &\cdot[(\alpha'^{(j)}\text{SOC}^{(j)}_{\max}+\beta'^{(j)})^{\frac{1}{z}+1} - (\alpha'^{(j)}\text{SOC}^{(j)}_{\min}+\beta'^{(j)})^{\frac{1}{z}+1}] \end{aligned} \tag{25}$$

For sake of brevity, define $\Lambda^{(j)} = \Lambda^{(j)}(\zeta, z)$ as

$$\Lambda^{(j)} \coloneqq \exp\left(\frac{-31700+\zeta I^{(j)}_c}{R_{gas}\theta z}\right), \tag{26}$$

and $\Gamma^{(j)} = \Gamma^{(j)}(\alpha'^{(j)}, \beta'^{(j)}, z)$ as

$$\begin{aligned}\Gamma^{(j)} \coloneqq &\frac{1}{\alpha'^{(j)}}\left[\left(\alpha'^{(j)}\text{SOC}^{(j)}_{\max}+\beta'^{(j)}\right)^{\frac{1}{z}+1}\right. \qquad (27)\\ &\left. - \left(\alpha'^{(j)}\text{SOC}^{(j)}_{\min}+\beta'^{(j)}\right)^{\frac{1}{z}+1}\right]. \qquad (28)\end{aligned}$$

Equating (21) with (25) results in the following equation.

$$\begin{aligned}(Q^{(j)}_{\text{rated}} - \mathcal{Q}^{(j)}_{k-1})^{\frac{1}{z}} - (Q^{(j)}_{\text{rated}} - \mathcal{Q}^{(j)}_{k})^{\frac{1}{z}} &= \frac{-2z}{(z+1)}\Lambda^{(j)}\Gamma^{(j)} \\ &\cdot \sum_{l=n^{(j)}_{k-1}+1}^{n^{(j)}_{k}} Q^{(j)}_{l,\max} \end{aligned} \tag{29}$$

Average value of $Q_{\max}$ during $\mathcal{I}^{(j)}_k$, $\tilde{Q}_{max,\mathcal{I}^{(j)}_k}$, can be approximated by $\sum_{l=n^{(j)}_{k-1}+1}^{n^{(j)}_{k}} Q^{(j)}_{l,\max}/\left(n^{(j)}_{k} - n^{(j)}_{k-1}\right)$. Additionally, it is assumed that r_j is large enough which in turn means $\mathcal{Q}^{(j)}_{k-1} - \mathcal{Q}^{(j)}_{k}$ is sufficiently small to approximate $\tilde{Q}_{max,\mathcal{I}^{(j)}_k}$ with $\left(\mathcal{Q}^{(j)}_{k-1} + \mathcal{Q}^{(j)}_{k}\right)/2$. This linear approximation implies

$$\frac{\sum_{l=n^{(j)}_{k-1}+1}^{n^{(j)}_{k}} Q^{(j)}_{l,\max}}{n^{(j)}_{k} - n^{(j)}_{k-1}} \approx \frac{\mathcal{Q}^{(j)}_{k-1} + \mathcal{Q}^{(j)}_{k}}{2} \tag{30}$$

Substituting the summation in (30) into (29) gets the equation $\text{e}^{(j)}_k$ for interval $\mathcal{I}^{(j)}_k$:

$$\begin{aligned}\text{e}^{(j)}_k : (Q^{(j)}_{\text{rated}} - \mathcal{Q}^{(j)}_{k-1})^{\frac{1}{z}} - (Q^{(j)}_{\text{rated}} - \mathcal{Q}^{(j)}_{k})^{\frac{1}{z}} &= \frac{-2z}{(z+1)}\Lambda^{(j)}\Gamma^{(j)} \\ &\cdot (n^{(j)}_{k} - n^{(j)}_{k-1})\frac{\mathcal{Q}^{(j)}_{k} + \mathcal{Q}^{(j)}_{k-1}}{2} \end{aligned} \tag{31}$$

Now consider equations $\text{e}'^{(j)}_k \coloneqq \sum_{s=1}^{k} \text{e}^{(j)}_s$, $k = 1, 2, \ldots r_j$:

$$\text{e}'^{(j)}_k : (Q^{(j)}_{\text{rated}} - \mathcal{Q}^{(j)}_{k})^{\frac{1}{z}} = \frac{2z}{(z+1)}\Lambda^{(j)}\Gamma^{(j)}\sum_{s=1}^{k}\Delta n^{(j)}_s \tilde{\mathcal{Q}}^{(j)}_s\,, \tag{32}$$

where $\Delta n^{(j)}_s \coloneqq n^{(j)}_s - n^{(j)}_{s-1}$ and $\tilde{\mathcal{Q}}^{(j)}_s \coloneqq \left(\mathcal{Q}^{(j)}_s + \mathcal{Q}^{(j)}_{s-1}\right)/2$. The idea is to first find z. For this, divide $\text{e}'^{(j)}_k$ by $\text{e}'^{(j)}_1$, for $k = 2, 3, \ldots r_j$, and then take the logarithm of both sides of the resulting equations to get

$$\log\left(\frac{1}{\Delta n^{(j)}_1 \tilde{\mathcal{Q}}^{(j)}_1}\sum_{s=1}^{k}\Delta n^{(j)}_s \tilde{\mathcal{Q}}^{(j)}_s\right) z = \log\left(\frac{Q^{(j)}_{\text{rated}} - \mathcal{Q}^{(j)}_{k}}{Q^{(j)}_{\text{rated}} - \mathcal{Q}^{(j)}_{1}}\right). \tag{33}$$

The only unknown parameter in (33) is z. Stacking equations (33) for $k = 2, 3, \ldots, r_j$, $j = 1, 2, \ldots, N$, and then using the least square method gives z.
Substituting z into (32) gets the value for $\Lambda^{(j)}\Gamma^{(j)}$:

$$\Lambda^{(j)}\Gamma^{(j)} = \frac{z+1}{2zr_j}\sum_{k=1}^{r_j}\frac{(Q^{(j)}_{\text{rated}} - \mathcal{Q}^{(j)}_{k})^{\frac{1}{z}}}{\sum_{s=1}^{k}\Delta n^{(j)}_s \tilde{\mathcal{Q}}^{(j)}_s} \tag{34}$$

α', β' and ζ are found by solving nonlinear equations (34), $j = 1, 2, \ldots, N$, by Matlab nonlinear equation solver. It

is important to set function tolerance small enough to derive accurate estimates. Also, if all experiments are performed at the same temperature, C-rates for at least two experiments have to be different so that ζ can be identified uniquely.

As it was mentioned earlier, assuming more distinct values for α' and β' requires more diverse experiments in terms of SOC window. For the present case study, similar structure for α' and β' is considered as in Suri and Onori (2016):

$$\alpha' = \begin{cases} \alpha'_1 & \text{SOC} \leq 0.45 \\ \alpha'_2 & \text{SOC} > 0.45 \end{cases} ; \beta' = \begin{cases} \beta'_1 & \text{SOC} \leq 0.45 \\ \beta'_2 & \text{SOC} > 0.45 \end{cases} \quad (35)$$

Data from 8 experiments are used for parameter identification. Experiments are diverse enough in C-rate, SOC and temperature such that all model parameters can be estimated. Identified parameters are presented in table (1). Figure (6) compares capacity loss prediction from resulting model and measured data for four experiments.

Table 1: Identified parameters for the model (17)

z	ζ	α'_1	α'_2	β'_1	β'_2
0.62	202.5	3758.1	3028.7	233.8	0

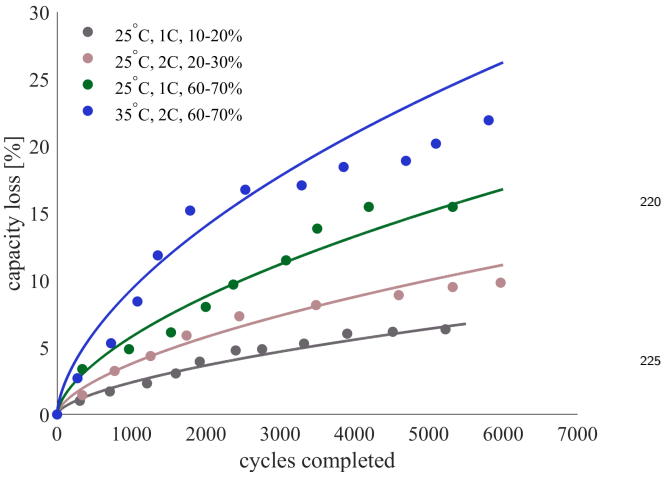

Figure 6: Capacity loss values from identified aging model (curves) versus measured capacity loss by RPT for four experiments.

Remark 1. In derivation of (20,25), it was assumed that the cycle is symmetric. Alternatively if $I^{(j)}_{c,\text{ch}} \neq I^{(j)}_{c,\text{dis}}$, right-hand-side of (20) must be replaced by

$$-z \sum_{l=n^{(j)}_{k-1}+1}^{n^{(j)}_k} \oint_{\mathcal{C}^{(j)}_l} \exp\left(\frac{-31700+\zeta I_c}{R_{gas}\theta z}\right)(\alpha' \text{SOC} + \beta')^{\frac{1}{z}}|I|\,\text{d}t \quad (36)$$

and it is straight-forward to show that a similar expression to (25) can be derived with the exponential term replaced by

$$\frac{1}{2}\left(\exp\left(\frac{-31700+\zeta I^{(j)}_{c,\text{ch}}}{R_{gas}\theta z}\right)+\exp\left(\frac{-31700+\zeta I^{(j)}_{c,\text{dis}}}{R_{gas}\theta z}\right)\right) \quad (37)$$

The rest of the procedure is similar.

Remark 2. Better estimates can be attained if vector of Ah-throughputs, $Ah^{(j)} = [Ah^{(j)}_0, Ah^{(j)}_1, \ldots, Ah^{(j)}_{r_j}]^T$, is available since it provides a better approximation for the summation in (29):

$$\begin{aligned} Ah^{(j)}_k - Ah^{(j)}_{k-1} &= \int_{t^{(j)}_{k-1}}^{t^{(j)}_k} |I(t)|\,\text{d}t \\ &= \left|I^{(j)}_c\right| \int_{t^{(j)}_{k-1}}^{t^{(j)}_k} Q_{\max}(t)\text{d}t \\ &\approx \left|I^{(j)}_c\right| t^{(j)}_{cyc} \sum_{l=n^{(j)}_{k-1}+1}^{n^{(j)}_k} Q^{(j)}_{l,\max} \end{aligned} \quad (38)$$

$\text{e}'^{(j)}_k$ then becomes

$$\text{e}'^{(j)}_k : (Q^{(j)}_{\text{rated}} - \mathcal{Q}^{(j)}_k)^{\frac{1}{z}} = \frac{2z}{(z+1)\left|I^{(j)}_c\right| t^{(j)}_{cyc}} \Lambda^{(j)}\Gamma^{(j)} Ah^{(j)}_k. \quad (39)$$

In this case, the assumption for large r_j, although desirable, is not as critical.

3. Energy management problem formulation

The main objective of the present paper is to design a control policy that fulfills two goals: reduction in fuel consumption and minimization of battery wear. Clearly, there is a trade-off between the two as less fuel consumption is achieved by increasing battery usage which accelerates aging of the battery. The policy should also sustain battery electric charge after a driving mission. Electric power demand for the hybrid electric wheel loader under consideration is often quite high and at times, surpass the maximum power that can be delivered by the genset. Existence of a high-power battery system can dramatically increase chances of saving fuel when such demands are requested by driver. Depletion of battery charge due to power assist can then be compensated for during episodes of braking that provide significant amount of power for recuperation. However, this approach cannot be applied as simply as stated since engine and battery operations during hybrid drive and regenerative braking modes affect the optimization objectives. Braking phases are frequent and not necessarily short in time. Therefore, regenerative braking is not addressed separately from hybrid drive by a different control policy. Solution is found through solving an optimal control problem which will be formulated in the sequel. Start-stop is dealt with separately since it is an instantaneous decision to make.

The first step to solving the energy management problem is to quantify the optimization objectives. The idea is to penalize fuel consumption and battery wear. Total amount of fuel consumed in a driving mission is given by

$$m_f(t_f) = \int_{t_i}^{t_f} \dot{m}_f \, \mathrm{d}t \,. \tag{40}$$

Battery wear can be incorporated into fuel economy measure (40) to construct a cost function that reflects upon both optimization objectives. Consider a differentiable, strictly increasing scalar function ϕ. A weighted sum of $m_f(t_f)$ and $\phi(Q_d(t_f))$ can be regarded as cost function for this purpose:

$$J = a_1 m_f(t_f) + a_2 \phi(Q_d(t_f)) \tag{41}$$

Minimizing (41) amounts to minimization of

$$J = \int_{t_i}^{t_f} \left(a_1 \dot{m}_f + a_2 \dot{Q}_d \frac{\mathrm{d}\phi}{\mathrm{d}Q_d} \right) \mathrm{d}t \,. \tag{42}$$

Weighting parameters (a_1, a_2) should be chosen such that fuel consumption and aging terms are comparable in terms of size and unit. One idea is to express J in terms of monetary costs (Serrao et al., 2011b). Fuel cost is computed by multiplying the mass of the fuel consumed by the cost per unit of fuel. For the battery, aging cost can be considered as the drive cycle's contribution to capacity degradation divided by the total degradation that marks battery's end of life (EOL). Battery is assumed to reach its end of life once its capacity reaches 80% of its nominal value. A candidate cost function is

$$J_m = m_f \xi_f + \frac{Q_d(t_f) - Q_d(t_i)}{Q_d^{EOL}} \xi_b \,, \tag{43}$$

in which ξ_f is fuel price per kg, ξ_b is the price of brand new battery pack, and Q_d^{EOL} denotes value of Q_d when battery reaches its end of life, i.e. $Q_d^{EOL} = (0.2 Q_{\mathrm{rated}})^{\frac{1}{z}}$. Corresponding values for (a_1, a_2) are given by

$$a_1 = \xi_f; \; a_2 = \frac{\xi_b}{Q_d^{EOL}} \left(\left(\frac{\mathrm{d}\phi}{\mathrm{d}Q_d} \right)_{t=t_f} \right)^{-1} . \tag{44}$$

It is worth underlying that as prices change with time, optimization results might not be valid anymore once new costs are registered. Another idea, employed by Tang et al. (2015), is to make fuel consumption and battery aging measures dimensionless through scaling. This approach makes the objective metrics comparable numerically. A similar idea is used in present paper. Corresponding values for (a_1, a_2) are

$$a_1 = \frac{a}{\dot{m}_{f,\mathrm{ref}}}; \; a_2 = \frac{1-a}{\mathcal{A}_{\mathrm{ref}} \left(\dfrac{\mathrm{d}\phi}{\mathrm{d}Q_d} \right)_{Q_{d,\mathrm{ref}}}} \,, \tag{45}$$

in which $\dot{m}_{f,\mathrm{ref}}$, $\mathcal{A}_{\mathrm{ref}}$ and $Q_{d,\mathrm{ref}}$ represent reference values. In (45), a takes values from 0 to 1 and determines "relative degree of importance" given to the two optimization objectives. To find the appropriate control policy, optimal control problem is solved by varying a from 0 to 1 and then the best value is chosen based on a criterion on optimal solutions.

In this work, $\phi(Q_d) = Q_d$, $\dot{m}_{f,\mathrm{ref}}$ is the maximum possible fuel mass flow rate and $\mathcal{A}_{\mathrm{ref}}$ is the maximum value $\mathcal{A}$ can attain in a drive cycle and is given by $\mathcal{A}_{\mathrm{ref}} = \mathcal{A}(1, I_{cyc,\max}, Q_{\mathrm{rated}})$. $I_{cyc,\max}$ is the maximum magnitude of battery current possible for the specific drive cycle. The reason for this choice is that in the wheel loader, $I_{cyc,\max}$ is considerably smaller than the nominal value $I_{\max}$ while it is normal for the engine to work at its nominal operating points.

The energy management problem is to minimize

$$J_{wl} = a_1 m_f(t_f) + a_2 Q_d(t_f), \tag{46}$$

with a_1,a_2 given by (45), subjected to dynamics (8),(16a), and the constraints

$$\begin{aligned} & W_{ech}(t_f) = W_{ech}(t_i) = W_{ech,i} \\ & W_{ech}(t) \in \mathcal{W}, \qquad t \in [t_i, t_f] \\ & P_b(t) \in \mathcal{P}_t \,. \end{aligned} \tag{47}$$

In the above, $\mathcal{W}$ and $\mathcal{P}_t$ represent sets of admissible state for W_{ech} and admissible input P_b at time t, respectively. $W_{ech,0}$ is taken as $U_{oc} Q_{\mathrm{rated}}/2$ and is required to be recovered by the end of the drive cycle.

4. Solution to the optimal control Problem

The energy management problem described in the previous section is solved by Pontryagin's minimum principle (PMP). The method is used to minimize the following integral cost function

$$J_p = \varphi(x(t_f), t_f) + \int_{t_i}^{t_f} L(x(t), u(t), t) \, \mathrm{d}t. \tag{48}$$

System's dynamics is given by

$$\dot{x} = f(x(t), u(t), t); \qquad x(t_i) = x_0, \tag{49}$$

where $u(t)$ and $x(t)$ lie in admissible sets $\mathcal{U}$ and $\mathcal{X}$, respectively, and $\varphi(x(t_f), t_f)$ is the final cost.

There are in general two types of constraints on the state. The first one corresponds to terminal condition on the state (global constraint) that can be either expressed as a hard constraint $\psi(x(t_f), t_f) = 0$ or be introduced smoothly into the cost function as an additive penalty, e.g., $\varphi(x(t_f), t_f)$ in (48), to account for deviations from the desirable terminal state. Second type of state constraints limits the state trajectory for $t \in [t_i, t_f]$ (local constraint), and can be represented by $h(x(t), t) \leq 0$.

The goal is to find an input $u^* \in \mathcal{U}$ that minimizes J_p among all admissible input signals. The corresponding state trajectory is found by simulating the dynamics with the initial condition $x(t_i) = x_0$, once the optimal control

input is known. For $h(x(t),t) < 0$, optimal solution can be found by minimizing the Hamiltonian defined by

$$\begin{aligned} H &= H(x(t),u(t),\lambda(t),t) \\ &:= L(x(t),u(t),t) + \lambda(t)^T f(x(t),u(t),t) \end{aligned} \tag{50}$$

at any instance. In (50), λ is the costate variable. Denoting the optimal trajectory and costate by $x^*(t)$ and $\lambda^*(t)$, respectively, the following holds for the optimal solution.

$$H(x^*(t),u^*(t),\lambda^*(t),t) \leq H(x^*(t),u(t),\lambda^*(t),t) \tag{51}$$

Time evolution of the costate is given by

$$\dot{\lambda}^*(t) = -\frac{\partial H}{\partial x} \tag{52}$$

Terminal boundary condition for λ is computed by (Bryson, 2018)

$$\lambda^*(t_f) = \left(\frac{\partial \varphi}{\partial x} + \frac{\partial \psi}{\partial x}\nu\right)_{t=t_f}, \tag{53}$$

where ν is such that $\psi(x(t_f),t_f) = 0$ holds. The set of differential equations described by (49),(52-53) poses a two-point boundary value problem. The initial value of the costate can be found by, for example, shooting methods (Bock and Plitt, 1984; Diehl et al., 2006; Diehl and ESAT-SCD, 2011).

5. Implementation of optimal controller for hybrid electric wheel loader

For the energy management problem, Hamiltonian (50) becomes

$$H = a_1 \dot{m}_f + \lambda_{ech}\dot{W}_{ech} + \lambda_{age}\dot{Q}_d \tag{54}$$

$\lambda = [\lambda_{ech}\ \lambda_{age}]^T$ is the costate vector and

$$a_1 = \frac{a}{\dot{m}_{f,\text{ref}}} \tag{55}$$

Costates' dynamics will be

$$\begin{aligned} \dot{\lambda}_{ech} &= -\frac{\partial H}{\partial W_{ech}} \\ &= -\lambda_{age}\frac{\alpha'}{zU_{oc}Q_{\max}}(\alpha'\text{SOC} + \beta')^{(\frac{1}{z}-1)} \\ &\cdot \exp\left(\frac{-31700 + \zeta\frac{|I|}{Q_{\max}(Ah)}}{R_{gas}\theta z}\right)|I|, \end{aligned} \tag{56}$$

and

$$\begin{aligned} \dot{\lambda}_{age} &= -\frac{\partial H}{\partial Q_d} \\ &= -\lambda_{age}\mathcal{A}\frac{Q_d^{z-1}}{(Q_{\text{rated}} - Q_d^z)^2} \\ &\cdot \left(\frac{\alpha' W_{ech}}{\beta' U_{oc} + \frac{\alpha' W_{ech}}{Q_{\text{rated}} - Q_d^z}} + \frac{\zeta|I|}{R_{gas}\theta}\right). \end{aligned} \tag{57}$$

In (56), dependency of current on state of charge is neglected for simplicity, but it can be taken into account as an implemented map.

According to (46,47), charge sustaining policy is formulated as a hard constraint on $W_{ech}(t_f)$, namely $\psi(x(t_f)) = W_{ech}(t_f) - W_{ech,i}$, and final cost is $\varphi(x(t_f),t_f) = a_2 Q_d(t_f)$ with $a_2 = (1-a)/\mathcal{A}_{\text{ref}}$. Boundary value conditions for costates are

$$\lambda_{ech}(t_f) = \nu_{ech}; \qquad \lambda_{age}(t_f) = a_2, \tag{58}$$

where ν_{ech} is a constant that guarantees charge sustenance.

5.1. Approximate solution to the optimal control problem

The partial derivative $\frac{\partial \dot{Q}_d}{Q_d}$ is depicted in figure (7) for the maximum possible battery current for all wheel loader drive cycles. Assuming $Q_d \neq 0$, the derivative is quite small even for a slightly worn battery. This means that $\dot{\lambda}_{age}$ is insignificant in practice. Thus, instead of solving the two-point boundary value problem described previously, a suboptimal alternative is to neglect dynamics of λ_{age} and treat it as a constant to simplify derivation of solution:

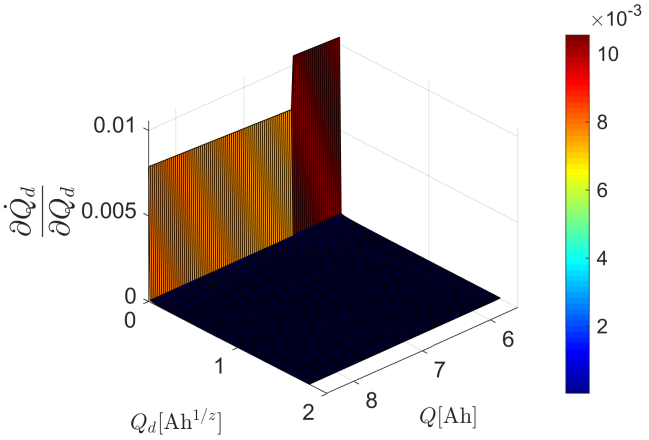

Figure 7: $\frac{\partial \dot{Q}_d}{Q_d}$ for $I \approx 300$A

$$\lambda_{age}(t) = \lambda_{age}(t_f) = a_2 \tag{59}$$

It will be shown in the next section that this approach alone improves battery life significantly while the paid price is a negligible increase in fuel consumption, compared to the case when aging is not considered ($a = 1$).

Remark 3. Since one of the objectives of the energy management strategy is to minimize battery wear in terms of capacity loss, it is more natural to directly embed capacity loss in the cost function (46) instead of Q_d, i.e. to minimize

$$J_{wl,2} = a_1{}' m_f(t_f) + a_2{}' Q_{loss}(t_f). \tag{60}$$

This corresponds to $\phi(Q_d(t_f)) = Q_d^z(t_f)$ in (41). In this case, approximating $\lambda_{age}(t)$ with its boundary condition is

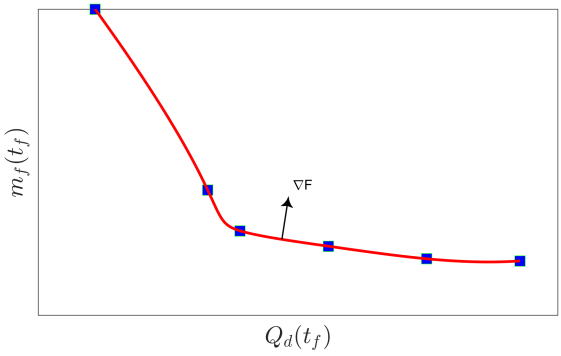

Figure 8: Pareto optimal curve $F(Q_d, m_f) = 0$ (red curve) plotted by solving the energy management problem for $a \in [0, 1]$. A few solution points are demonstrated in blue squares.

not as desireable because $\lambda_{age}(t_f)$ depends on final state $Q_d(t_f)$ which is not known a priori (as opposed to (59)):

$$\lambda_{age}(t_f) = zQ_d^{z-1}(t_f) \tag{61}$$

It can be shown that optimizing cost functions (46) and (60) are indeed equivalent in that they lead to the same Pareto optimality results, provided that a certain relation between (a_1, a_2) and $(a_1{}', a_2{}')$ is satisfied. Pareto front for the optimization problem defined by cost function (46) and constraints (47) can be found by varying a from 0 to 1 in (55). The result is the curve $F(Q_d, m_f) = 0$ shown in figure (8). Similarly, Pareto front $G(Q_{loss}, m_f) = 0$ can be achieved if (60) is used as the cost function. For any point (Q_{loss}, m_f) on G, $(Q_{loss}^{1/z}, m_f)$ is on F due to optimality of solutions. In other words,

$$G(Q_{loss}, m_f) = F(Q_{loss}^{1/z}, m_f). \tag{62}$$

Now, suppose that (Q_{loss}^*, m_f^*) is on G and corresponds to coefficients $(a_1'^*, a_2'^*)$. Then $({Q_{loss}^*}^{1/z}, m_f^*)$ must be on F, corresponding to a couple (a_1^*, a_2^*). Gradient of G at (Q_{loss}^*, m_f^*) is normal to G at that point and is given by (Boyd et al. (2004))

$$\nabla G(Q_{loss}^*, m_f^*) = \begin{bmatrix} a_1'^* \\ a_2'^* \end{bmatrix} \tag{63}$$

Similarly,

$$\nabla F({Q_{loss}^*}^{1/z}, m_f^*) = \begin{bmatrix} a_1^* \\ a_2^* \end{bmatrix} \tag{64}$$

From (62),

$$\frac{\partial G}{\partial Q_{loss}}(Q_{loss}^*, m_f^*) = \frac{1}{z}{Q_{loss}^*}^{(1/z)-1}\frac{\partial F}{\partial Q_d}({Q_{loss}^*}^{1/z}, m_f^*), \tag{65a}$$

$$\frac{\partial G}{\partial m_f}(Q_{loss}^*, m_f^*) = \frac{\partial F}{\partial m_f}({Q_{loss}^*}^{1/z}, m_f^*), \tag{65b}$$

which together with (63, 64) give

$$a_1^* = z{Q_{loss}^*}^{(1-1/z)}a_1'^*, \tag{66a}$$

$$a_2^* = a_2'^*. \tag{66b}$$

Thus, minimizing the cost function (46) with (a_1^*, a_2^*), calculated by (66), yields the same result as using (60) with $(a_1'^*, a_2'^*)$. Corresponding value for a can be found through solving (45).

5.2. Regenerative braking and start-stop functionality

In the ideal scenario where there is no aging phenomena, it is optimal to regenerate as much power as possible during braking periods. This, however, does accelerate aging processes as battery aging model does not discriminate between charge and discharge currents. Thus, it is important to consider this issue while finding the optimal inputs. Also, to maintain optimality of solution, one cannot address regenerative braking separately from traction mode since braking phases can be considerably long.

A properly designed start-stop policy helps to reduce emissions, noise and fuel consumption by eliminating unnecessary idling times. To accomplish this, it is assumed that engine is on when both power request from driver and genset's output power, which is determined by the controller, are positive, and it is shut off otherwise. Minimization of number of on/off switchings is not considered in this paper, but it can be added to objectives of the energy management problem.

6. Case Study

Performance of the proposed control strategy is examined by numerous simulations, a few of which are presented in this section. Four main drive cycles, namely short loading cycle (SLC), fork palletizing (FP), load and carry (LC), and load and carry uphill (LCU), are chosen to predict how well energy management objectives are achieved for the wheel loader. It is difficult to assess control strategy's performance based on simulation of only one drive cycle since 1) change in battery's maximum capacity is infinitesimal after one drive cycle and 2) differences in final values of battery electric charge, however slight, can make comparisons impossible. Thus, long duration simulations are carried out and their results are discussed. Still, short-term simulations are worthwhile to shed light upon how differently the vehicle operates when the new strategy is implemented compared to the case where betterment of fuel economy is the only optimization goal ($a = 1$). These cases will be referred to as *battery health-aware* and *fuel-only* scenarios, respectively.

6.1. Short-term simulations

To fulfill charge sustaining requirement, battery electrochemical energies in the beginning and at the end of a drive cycle have to be the same. In electric charge terms, each drive cycle starts with $Q^{t_i} = Q(0) = 0.5Q_{\text{rated}}$ and should end up with $Q(t_f) \in [Q^{t_i}(1-\delta)\ Q^{t_i}(1+\delta)]$, in which δ designates maximum allowed relative tolerance. In this work, $\delta = 0.01$ is chosen. Secant method is used to

determine $\lambda^*_{ech}(0)$ (Xie et al., 2017). The algorithm is initialized by simulating the control system with two preset values λ^0_0, λ^0_1 for $\lambda_{ech}(0)$ to find corresponding final electric charges $Q^{t_f}_0$,$Q^{t_f}_1$, respectively. Initial value of the optimal costate is found by the iteration

$$\lambda^0_j = \lambda^0_{j-1} - \left(\lambda^0_{j-1} - \lambda^0_{j-2}\right) \frac{Q^{t_f}_{j-1} - Q^{t_i}}{Q^{t_f}_{j-1} - Q^{t_f}_{j-2}}, \qquad (67)$$

for $j = 2, 3, \ldots, j_{\max}$ in which $Q^{t_f}_j$ is the final electric charge resulting from $\lambda_{ech}(0) = \lambda^0_j$. Algorithm stops if either maximum number of iterations $j_{\max}$ is reached or $Q(t_f)$ is within the specified bounds.

For each drive cycle, two cases are considered; fuel-only ($a = 1$) and a battery health-aware case ($a \neq 1$). Optimal battery power for each scenario is depicted in figure (9). To elucidate differences between control policies, optimal battery power signals, classified based on wheel loader's modes of operation - namely regenerative braking, battery recharging and power assist modes - are indicated in figure (10) for SLC, FP and LCU drive cycles. Optimal state of charge and costate trajectories are demonstrated in figure (11) and (12), respectively. Following observations are made for battery health-aware case compared to fuel-only case:

(i) The battery does not always recuperate all provided power during regenerative braking. In particular, for SLC and FP, brake power is fully recuperated, but for LC and LCU, recuperation is not perfect at times. On the contrary, for fuel-only case, regenerated power is limited just by battery's maximum charging power. Otherwise, it regenerates as much as provided. It should be noted that even for LC and LCU, the two scenarios do not result in much different behavior during recuperation. For rule-based realization of the policy, this implies that control of this mode might be implemented the same way as for fuel-only case.

(ii) Charging power is usually smaller during battery recharging mode. This can be clearly seen from initial phases of all power cycles shown in figure (9) and for all cases in figure (10). The most extreme case occurs for FP, where battery recharging mode is almost nonexistent (very small charge power). In this case, the vehicle might even be in power assist mode with a relatively small discharge rate while it would operate in battery recharging mode for the fuel-only case. Also, the battery tends to help less during power assist for $a \neq 1$. This implies that reducing a results in a "charge less, assist less" attitude of the battery. This behavior does not automatically mean that the wheel loader spends less time in charging or assist modes. For instance, for FP, the duration of assist mode becomes longer as a decreases.

(iii) Figure (12) suggests that relative variations in λ_{ech} from its initial value are very small for one drive cycle. A simplified solution is thus to consider it constant for one drive cycle. Of course, the costate's initial value has to be updated for subsequent drive cycles regardless of applying such simplification.

(iv) Improvements in battery life can be achieved by decreasing absolute value of battery current and/or by pushing state of charge trajectory towards values for which aging intensity factor becomes small (see equation (15)). According to figure (13), the latter takes place if state of charge gets as close to 0.45 as possible for SOC > 0.45. From figure (11), it can be seen that for LC and LCU, state of charge trajectories corresponding to the proposed strategy almost always lie beneath that of fuel-only solution, which is not the case for SLC and FP. This can be explained by the fact that LC and LCU are more "aggressive", in terms of power demand, than SLC and FP and there is less freedom to manipulate battery power during traction. Improving capacity loss will then take place by reducing state of charge rather than current's magnitude.

6.2. Long-term simulations

To simulate one day of operation, each drive cycle is repeated for 8 hours. One year of operation is considered to be equal to 365 one-day simulations by assuming linear scalability of Q_d and m_f, i.e.

$$\Delta Q^{\text{year}}_d = 365 \times \Delta Q^{\text{day}}_d, \qquad (68)$$

$$m^{\text{year}}_f = 365 \times m^{\text{day}}_f. \qquad (69)$$

6.2.1. λ adaptation

Initial value of the costate λ_{ech} has to be reset after a single standard drive cycle. For the values computed by iteration (67), final battery electric charge inevitably deviates from target electric charge for a single drive cycle. If the same value is used for $\lambda_{ech}(0)$ consecutively (for the same cycle), as for 8-hour simulation, the error will accumulate and grow large over time. Eventually, the battery either discharges completely or gets over-charged, for which the charge sustaining policy is violated in both cases. Additionally, maximum capacity fades over time and the battery ends up with more charge if the same initial costate value is used. In this work, dependence of $\lambda^*_{ech}(0)$ on initial electric charge and maximum capacity is implemented as a look-up table in Matlab:

$$\lambda^*_{ech}(0) = F_\lambda(Q^{t_i}, Q^{t_i}_{\max}) \qquad (70)$$

For any drive cycle, given initial values of battery charge and maximum capacity, $\lambda^*_{ech}(0)$ is calculated by linear interpolations using the map (70).

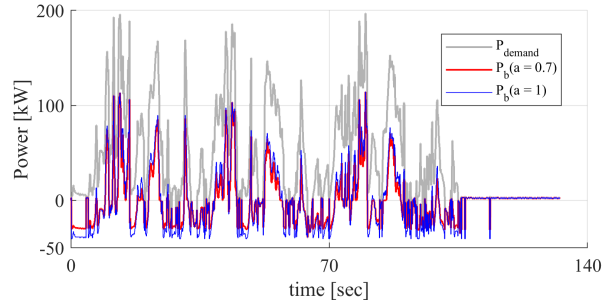

(a) Short loading cycle, $a = 0.7, 1$

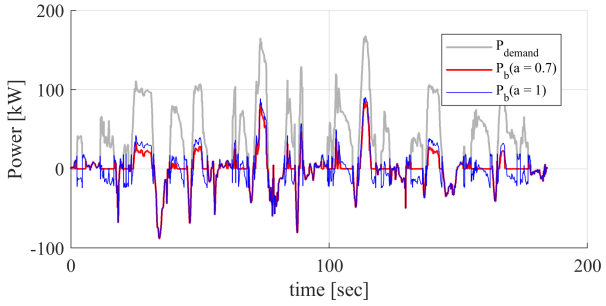

(b) Fork palletizing, $a = 0.7, 1$

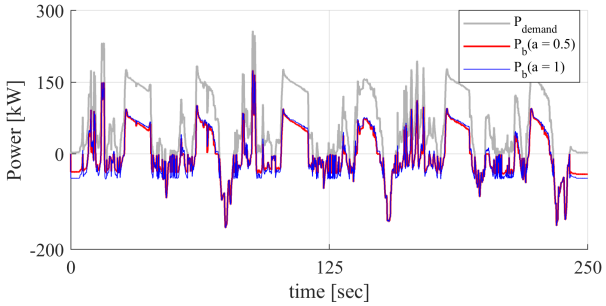

(c) Load and carry, $a = 0.5, 1$

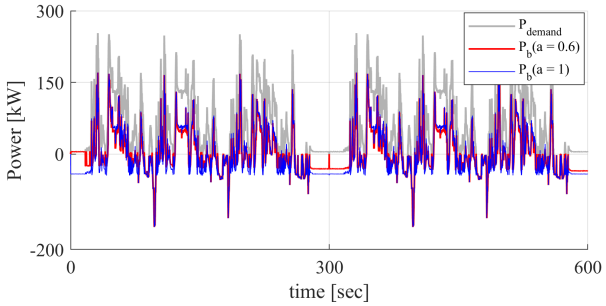

(d) Load and carry uphill, $a = 0.6, 1$. Only half of the cycle is illustrated.

Figure 9: Comparison between optimal battery powers for $a \neq 1$ (red lines) and $a = 1$ (blue lines). Electric power demand at the output of inverter is shown in gray.

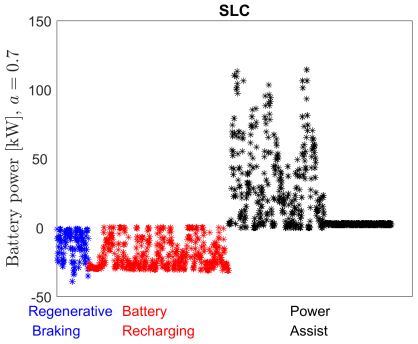

(a) Short loading cycle

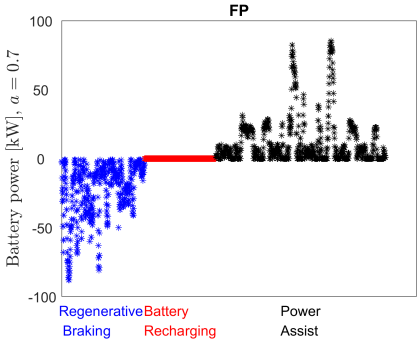

(b) Fork palletizing

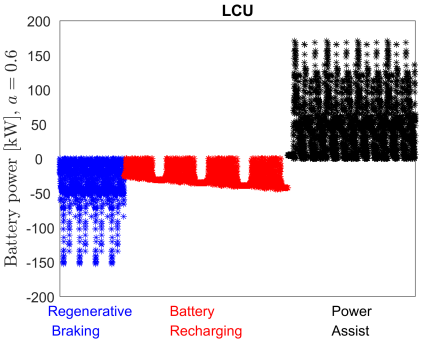

(c) Load and carry uphill

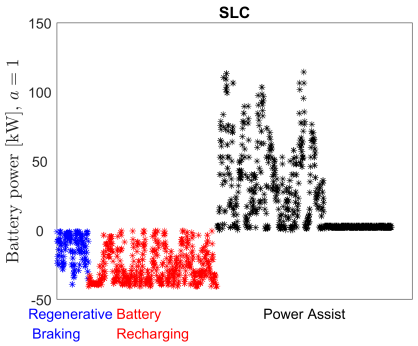

(d) Short loading cycle

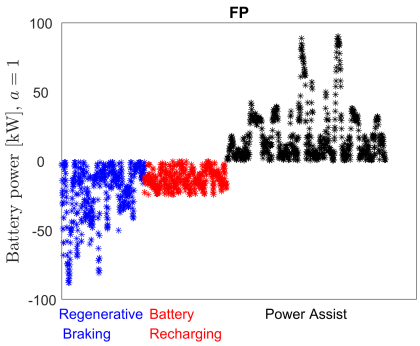

(e) Fork palletizing

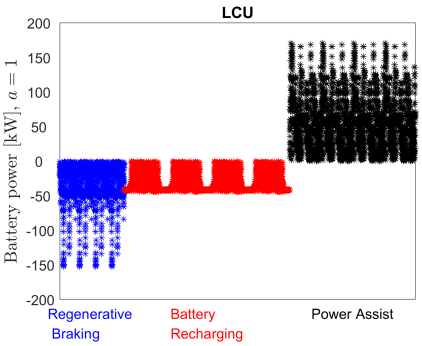

(f) Load and carry uphill

Figure 10: Battery power during different modes of wheel loader. (a,b,c): optimal solution for $a \neq 0$, (d,e,f): optimal solution for $a = 1$.

6.2.2. simulation results

After finding optimal fuel consumption and remaining battery capacity for one-day (one-year) operation of each drive cycle for $a = (0.1, 0.2, \ldots, 1)$, the best value for a, a_{opt}, is chosen based on a virtual cost function that roughly compares costs associated with the two energy

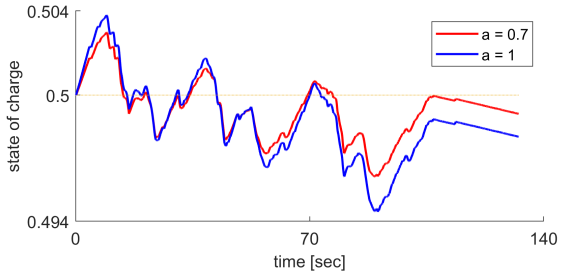

(a) Short loading cycle, $a = 0.7, 1$

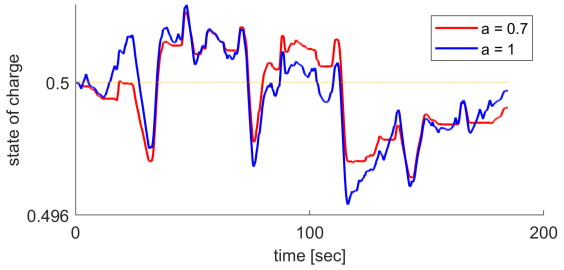

(b) Fork palletizing, $a = 0.7, 1$

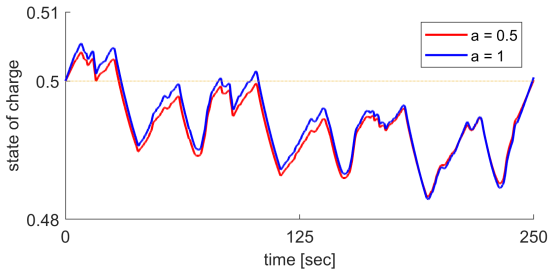

(c) Load and carry, $a = 0.5, 1$

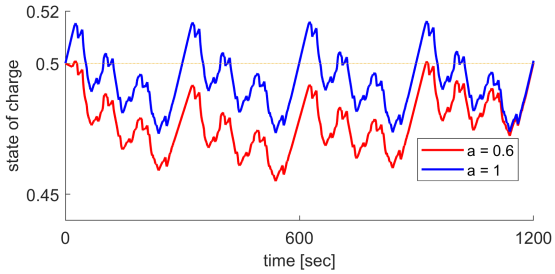

(d) Load and carry uphill, $a = 0.6, 1$

Figure 11: Optimal SOC trajectories for $a \neq 1$ (red lines) and $a = 1$ (blue lines).

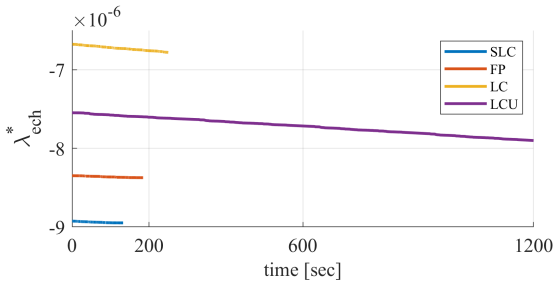

Figure 12: Optimal trajectories of costate λ_{ech} for $a \neq 1$

sources, namely diesel fuel and the lithium-ion battery.

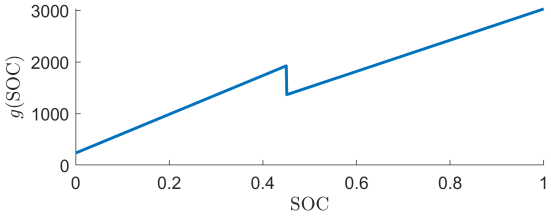

Figure 13: Dependency of $\mathcal{A}$ on SOC according to $g(\text{SOC}) = \alpha'\text{SOC} + \beta'$.

The proposed cost function is

$$J_v = \frac{m_f^{\text{year}}}{\rho_f}\bar{\xi}_f + \frac{\tilde{Q}_{loss}^{\text{year}}}{0.2Q_{\text{rated}}}\bar{\xi}_b\,, \tag{71}$$

in which m_f^{year} is the mass of fuel consumed in a year, ρ_f is density of diesel, $\tilde{Q}_{loss}^{\text{year}}$ is the average yearly capacity loss, $\bar{\xi}_f$ is the total cost corresponding to consumption of 1 liter of fuel, and $\bar{\xi}_b$ is the total cost associated with the battery system that includes the original price, maintenance costs, etc. Improvements in battery life and increase in fuel consumption compared to the fuel-only objective are presented in table (2). $\Delta T_{EOL}(\%)$ shows improvement in battery life (in percentage), $\Delta m_f(\%)$ is increase in fuel consumption (in percentage), and RMS denotes root mean square of drive cycles' power demands.

Table 2: Long term simulation results

Drive cycle	a_{opt}	$\Delta T_{EOL}(\%)$	$\Delta m_f(\%)$	RMS (kW)
SLC	0.7	+28.07	+0.34	64.9
FP	0.7	+55.35	+0.74	54.92
LC	0.5	+13.46	+0.21	92.05
LCU	0.6	+16.66	+0.3	84.60

It can be seen that for all cases, extension of battery's end of life relative to expense of a negligible increase in fuel consumption is significant. The largest relative increase in battery life is achieved for FP, followed by SLC, LCU and LC. Interestingly, this inversely correlates with root mean square of drive cycles' power demand. Normalized maximum capacities for LC and FP, over first year of usage, are shown in figure (14). In both cases, rate of capacity fade is reduced, but the improvement is conspicuously larger for FP.

In order to compare control policy's performance for different drive cycles, one may consider increase in battery life relative to extra fuel consumed:

$$\kappa = \frac{\Delta T_{EOL}(\text{year})}{\Delta m_f(\text{kg})} \tag{72}$$

Larger κ suggests a better performance. Corresponding values of κ are given in table (3). The same negative correlation between performance and RMS is observed as before.

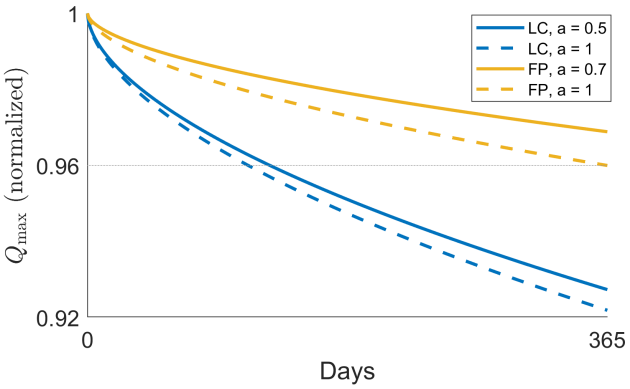

Figure 14: Capacity degradation over first year. Battery health-aware (dashed lines) versus fuel-only (solid lines)

Table 3: Values of κ.

Drive cycle	a_{opt}	κ	RMS (kW)
SLC	0.7	11.9537	64.9
FP	0.7	22.9403	54.92
LC	0.5	3.3003	92.05
LCU	0.6	3.5689	84.60

These results imply that there is more opportunity to prolong battery life while sacrificing small amount of fuel if the driving mission is less demanding. Hence, the proposed strategy works best for least aggressive drive cycles. This conclusion, nevertheless, is not surprising since fulfillment of power request from driver is primary to minimization of energy management indices, and when power requests are very high, there is less freedom for control system to improve desirable objectives.

7. Conclusion and Future Work

In this paper, battery health optimization was incorporated into the energy management problem using optimal control framework. The first step was to introduce and employ a differential algebraic model to simulate capacity loss in varying operational conditions. An identification method was proposed to identify the model parameters. The trade-off between fuel economy and capacity loss minimization was discussed in order to construct an appropriate cost function. Pontryagin's minimum principle was used to solve the optimal control problem. It was shown that the costate corresponding to capacity degradation dynamics is fairly constant so that the derivation of solution can be simplified to evolution of only one costate. Short-term simulations revealed that mitigating rate of capacity loss as a side objective causes battery to help less during assist mode and also charge less during battery-recharging/regenerative braking periods. Long-term simulations demonstrated that there is huge potential in enhancing battery life while not sacrificing fuel economy as the chief measure. Particularly for the wheel loader under study, increase in fuel consumption is negligible compared to the prolonged battery life. The method is especially promising when the driving mission is not aggressive in sense of power requirement.

Investigations performed in this paper can be done for other hybrid electric heavy-duty machinery. Future work entails studying practical implications of the proposed strategy. Specifically, it is of interest to (1) assess robustness of the control system against discrepancies between real-life and ideal drive cycles and (2) develop an adaptive version of the proposed methodology.

Acknowledgment

The authors want to thank Swedish Energy Agency for funding the project, and Volvo Construction Equipment for technical support throughout the project.

References

Bock, H.G., Plitt, K.J., 1984. A multiple shooting algorithm for direct solution of optimal control problems. IFAC Proceedings Volumes 17, 1603–1608.

Boyd, S., Boyd, S.P., Vandenberghe, L., 2004. Convex optimization. Cambridge university press.

Bryson, A.E., 2018. Applied optimal control: optimization, estimation and control. Routledge.

Diehl, M., Bock, H.G., Diedam, H., Wieber, P.B., 2006. Fast direct multiple shooting algorithms for optimal robot control, in: Fast motions in biomechanics and robotics. Springer, pp. 65–93.

Diehl, M., ESAT-SCD, K., 2011. Numerical optimal control draft.

Ebbesen, S., Elbert, P., Guzzella, L., 2012. Battery state-of-health perceptive energy management for hybrid electric vehicles. IEEE Transactions on Vehicular technology 61, 2893–2900.

Fröberg, A., Åslund, J., Nielsen, L., 2011. Optimal transient control of power generation in hybrid construction equipment, in: 2011 IEEE Vehicle Power and Propulsion Conference, IEEE. pp. 1–6.

Groot, J., 2012. State-of-health estimation of li-ion batteries: Cycle life test methods .

Guzzella, L., Sciarretta, A., et al., 2007. Vehicle propulsion systems. volume 1. Springer.

Huang, Y., Wang, H., Khajepour, A., He, H., Ji, J., 2017. Model predictive control power management strategies for hevs: A review. Journal of Power Sources 341, 91–106.

Jin, X., Vora, A., Hoshing, V., Saha, T., Shaver, G., Wasynczuk, O., Varigonda, S., 2018. Applicability of available li-ion battery degradation models for system and control algorithm design. Control Engineering Practice 71, 1–9.

Kim, N., Rousseau, A., 2012. Sufficient conditions of optimal control based on pontryagin's minimum principle for use in hybrid electric vehicles. Proceedings of the Institution of Mechanical Engineers, Part D: Journal of Automobile Engineering 226, 1160–1170.

Li, T., Liu, H., Ding, D., 2018. Predictive energy management of fuel cell supercapacitor hybrid construction equipment. Energy 149, 718–729.

Musardo, C., Rizzoni, G., Guezennec, Y., Staccia, B., 2005. A-ecms: An adaptive algorithm for hybrid electric vehicle energy management. European Journal of Control 11, 509–524.

Nilsson, T., Fröberg, A., Åslund, J., 2015. Predictive control of a diesel electric wheel loader powertrain. Control Engineering Practice 41, 47–56.

Nüesch, T., Wang, M., Isenegger, P., Onder, C.H., Steiner, R., Macri-Lassus, P., Guzzella, L., 2014. Optimal energy management for a diesel hybrid electric vehicle considering transient pm and quasi-static nox emissions. Control Engineering Practice 29, 266–276.

Onori, S., Serrao, L., Rizzoni, G., 2010. Adaptive equivalent consumption minimization strategy for hybrid electric vehicles, in: ASME 2010 dynamic systems and control conference, American Society of Mechanical Engineers Digital Collection. pp. 499–505.

Onori, S., Serrao, L., Rizzoni, G., 2016. Hybrid electric vehicles: Energy management strategies. Springer.

Padovani, T.M., Debert, M., Colin, G., Chamaillard, Y., 2013. Optimal energy management strategy including battery health through thermal management for hybrid vehicles.

Payri, F., Guardiola, C., Pla, B., Blanco-Rodriguez, D., 2014. A stochastic method for the energy management in hybrid electric vehicles. Control Engineering Practice 29, 257–265.

Pérez, L.V., Bossio, G.R., Moitre, D., García, G.O., 2006. Optimization of power management in an hybrid electric vehicle using dynamic programming. Mathematics and Computers in Simulation 73, 244–254.

Petit, M., Prada, E., Sauvant-Moynot, V., 2016. Development of an empirical aging model for li-ion batteries and application to assess the impact of vehicle-to-grid strategies on battery lifetime. Applied energy 172, 398–407.

Pham, T.H., Kessels, J.T., Van Den Bosch, P.P., Huisman, R.G., 2015. Analytical solution to energy management guaranteeing battery life for hybrid trucks. IEEE Transactions on Vehicular Technology 65, 7956–7971.

Prada, E., Petit, M., 2013. Aging modeling for advanced li-ion battery pack sizing and management for hev/ev through amesim simulation platform, in: LMS European vehicle conference, pp. 29–30.

Rezaei, A., Burl, J., Solouk, A., Zhou, B., Rezaei, M., Shahbakhti, M., 2017. Catch energy saving opportunity (ceso), an instantaneous optimal energy management strategy for series hybrid electric vehicles. Applied Energy 208, 655–665.

Sabri, M., Danapalasingam, K., Rahmat, M., 2016. A review on hybrid electric vehicles architecture and energy management strategies. Renewable and Sustainable Energy Reviews 53, 1433–1442.

Sciarretta, A., di Domenico, D., Pognant-Gros, P., Zito, G., 2014. Optimal energy management of automotive battery systems including thermal dynamics and aging, in: Optimization and optimal control in automotive systems. Springer, pp. 219–236.

Serrao, L., Onori, S., Rizzoni, G., 2011a. A comparative analysis of energy management strategies for hybrid electric vehicles. Journal of Dynamic Systems, Measurement, and Control 133.

Serrao, L., Onori, S., Sciarretta, A., Guezennec, Y., Rizzoni, G., 2011b. Optimal energy management of hybrid electric vehicles including battery aging, in: Proceedings of the 2011 American control conference, IEEE. pp. 2125–2130.

Sivertsson, M., Sundström, C., Eriksson, L., 2011. Adaptive control of a hybrid powertrain with map-based ecms. IFAC Proceedings Volumes 44, 2949–2954.

Spagnol, P., Onori, S., Madella, N., Guezennec, Y., Neal, J., . Aging and characterization of li-ion batteries in a hev application for lifetime estimation.

Suri, G., Onori, S., 2016. A control-oriented cycle-life model for hybrid electric vehicle lithium-ion batteries. Energy 96, 644–653.

Tang, L., Rizzoni, G., 2016. Energy management strategy including battery life optimization for a hev with a cvt, in: 2016 IEEE Transportation Electrification Conference and Expo, Asia-Pacific (ITEC Asia-Pacific), IEEE. pp. 549–554.

Tang, L., Rizzoni, G., Onori, S., 2014. Optimal energy management of hevs with consideration of battery aging, in: 2014 IEEE Conference and Expo Transportation Electrification Asia-Pacific (ITEC Asia-Pacific), IEEE. pp. 1–6.

Tang, L., Rizzoni, G., Onori, S., 2015. Energy management strategy for hevs including battery life optimization. IEEE transactions on Transportation Electrification 1, 211–222.

Wang, J., Liu, P., Hicks-Garner, J., Sherman, E., Soukiazian, S., Verbrugge, M., Tataria, H., Musser, J., Finamore, P., 2011. Cycle-life model for graphite-lifepo4 cells. Journal of power sources 196, 3942–3948.

Xie, S., Li, H., Xin, Z., Liu, T., Wei, L., 2017. A pontryagin minimum principle-based adaptive equivalent consumption minimum strategy for a plug-in hybrid electric bus on a fixed route. Energies 10, 1379.

Zhang, W., Wang, J., Du, S., Ma, H., Zhao, W., Li, H., 2019. Energy management strategies for hybrid construction machinery: Evolution, classification, comparison and future trends. Energies 12, 2024.